Exploring the Role of Thermodynamic Parameters in Determining Zr–Cu–Al–Ag Glass-Forming Composition

JUHI VERMA, SAI PRANAV, ABHILASHA JAIN, and JATIN BHATT

A new glass-forming composition (GFC) has been proposed in the Zr–Cu–Al–Ag system using thermodynamic modelling. Enthalpy of chemical mixing (ΔH_{chem}) and mismatch entropy ($\Delta S_\sigma/k_B$) is used along with configurational entropy ($\Delta S_c/R$) to optimize the GFC. In the present work, a novel computational calculation method is introduced on behalf of a graphical approach to accurately determine GFCs using the aforementioned thermodynamic parameters. Systematically quaternary Zr–Cu–Al–Ag system is subdivided into ternary systems to determine P_{HS} (ΔH_{chem}*$\Delta S_\sigma/k_B$) and P_{HSS} (P_{HS}*$\Delta S_c/R$) parameters. The P_{HSS} parameter is critically compared with reported Zr–Cu–Al–Ag BMGs. Based on the computational approach a new composition, $Zr_{47}Cu_{40}Al_8Ag_5$, is determined which is found to closely match with earlier reported metallic glasses. The role of varying Ag concentration from 1 to 8 at. pct has been analysed to understand the stability in GFCs. A thermodynamic analysis is also endeavoured to further explore the role of binary pairs on ΔH_{chem}, $\Delta S_\sigma/k_B$, $\Delta S_c/R$, P_{HS}, and P_{HSS} in this work.

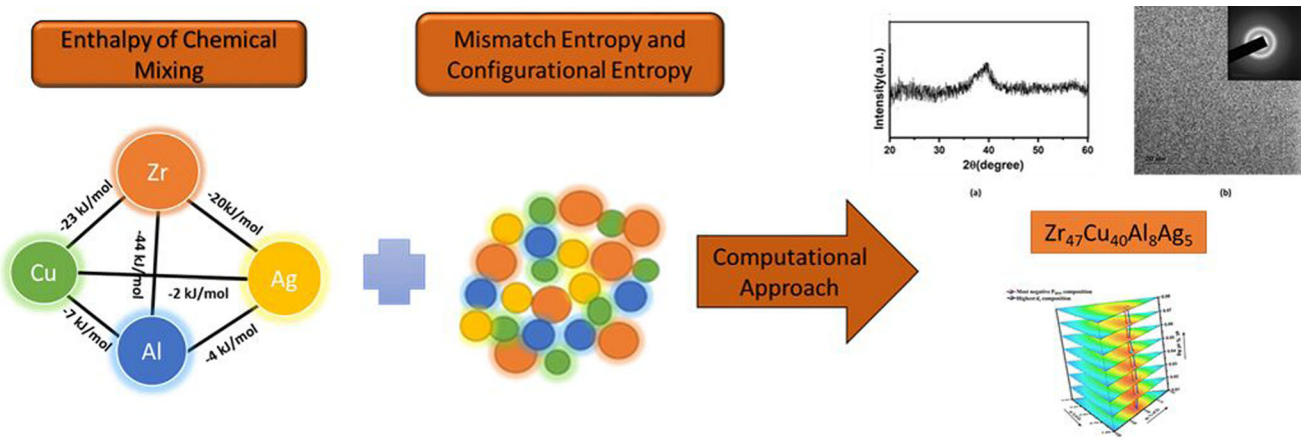

https://doi.org/10.1007/s11661-024-07339-2

I. INTRODUCTION

BULK Metallic Glasses (BMGs) are the amorphous solids formed by the rapid cooling from the liquid state and are characterized by their glass-forming ability (GFA). GFA suggests how easily vitrification of metallic liquid can be achieved without crystallisation.[1–3] Significant research has been conducted to predict the formation of BMGs in metallic systems, and several criteria have been formulated to predict the GFA.[4–8]

JUHI VERMA, SAI PRANAV, ABHILASHA JAIN, and JATIN BHATT are with the Department of Metallurgical and Materials Engineering, Visvesvaraya National Institute of Technology, Nagpur 440010, India. Contact e-mail: jverma146@gmail.com
Manuscript submitted September 21, 2023; accepted January 23, 2024.
Article published online February 28, 2024

The ratio of T_g/T_m is an important criterion established by Turnbull[9] to quantitatively estimate the GFA of any composition, where T_g and T_m are the glass transition and melting temperature, respectively.[9] It was predicted by Turnbull that the liquid melt with a ratio $T_g/T_m \leq 2/3$ can be an excellent glass former with a low critical cooling rate.[7] However, there are reports which suggest that T_{rg} is not an effective parameter to judge GFA for all the glass-forming systems.[10,11] Further, various other potential glass-forming parameters like ΔT_x,[12] γ,[13] α and β[14] were also developed to predict the GFA in BMG forming alloys. However, these parameters are based on experimentally verified thermal events that have been observed when glass is heated from room to elevated temperature under a controlled atmosphere in the calorimeter. Alternatively, the prediction of glass-forming composition (GFC) in metallic systems can also be achieved using the P_{HS} approach, considering thermodynamic parameters like enthalpy of chemical mixing (ΔH_{chem}) and mismatch entropy ($\Delta S_\sigma/k_B$).[15]

P_{HS} parameter is the product of ΔH_{chem} and $\Delta S_\sigma/k_B$. The P_{HS} criterion is centred on design principles, earlier proposed by Inoue[16] and Greer[17] and is effectively used to predict GFCs in various alloy systems.[18] Though, the exact mechanism of glass formation is unclear but the precise mechanisms and the interplay of various factors that contribute to glass formation in metallic systems are still under investigation. The empirical rules suggested by Inoue[16] are the guidelines to predict the new metallic glass composition. The three rules say that : (1) For the system to be viable, it must comprise a minimum of three components or more. As the number of components increases, the formation of metallic glasses should become easier. Multi-components can enhance the degree of random packing of the atoms in the system, resulting in higher fusion entropy and lower Gibbs free energy. This criterion is also in line with Greer's proposed ''confusion principle''.[17] (2)The elements used should have an atomic size difference of at least 12 pct. The density of random packing atoms can be increased by combining atoms with considerable differences in atomic sizes, which increases the viscosity of the alloy liquid and retards the atomic diffusion in the undercooled liquid, enhancing the glass formation. (3)The enthalpy of mixing should be negative. Negative mixing heat helps in the stabilisation of an undercooled liquid and the formation of a homogenous glassy state. This criterion helps in glass formation as a consequence of the efficient random packing of atoms. Since Inoue's empirical criteria are followed in a large number of reported BMGs, the aforementioned laws can be used as normative guidelines to forecast the potential GFCs.

P_{HSS} parameter, which can be defined as the product of P_{HS} and configurational entropy normalised by the Universal gas constant, serves as a promising metric for predicting glass formation. This parameter incorporates both topological and thermodynamic considerations, aligning with Inoue's three empirical rules and demonstrates its efficacy in discerning glass-forming tendencies of the liquid melt. In the liquid stage, the alloy system satisfying Inoue's three empirical laws shows efficient atomic packing and thus kinetically frustrating the formation of crystalline phase. The increase in viscosity hampers the atomic mobility, which results in effectively inhibiting the nucleation of the crystalline phase. This causes the liquid melt to stabilise at low temperatures, *i.e.,* to 'configurationally freeze' into a glassy phase when cooled.[19]

The metallic glass compositions are formed around deep eutectic regions in binary phase diagrams due to their lower melting point and stable liquid phase.[20] However, locating eutectic points in ternary, quaternary, and other higher-order systems is difficult and therefore pinpointing the GFC is challenging in such systems. Hence, the P_{HS} parameter is introduced to locate the Glass-forming region for the potential GFCs. Earlier, P_{HS}[21] was used for the ternary system, and a P_{HSS} was considered for quaternary or higher-order systems.[22] As the higher-order system includes more elements, they often have chemical and topological similarity and this limits the applicability of P_{HS}. In such a case, the inclusion of configurational entropy term in P_{HS} results in the P_{HSS} parameter that approximates the window for glass formation for higher-order systems.[23] On the other hand, more elements increase the confusion among energetically competitive phases and result in glass formation often with higher GFA.[24] In the present study, an easy and fast calculation method is introduced to pinpoint GFC in the Zr–Cu–Al–Ag BMG system employing a thermodynamic modelling approach. The P_{HSS} approach is widely accepted throughout and is used to predict the glass-forming compositions. P_{HSS} approach has been successfully used earlier for Zr,[25] Cu,[26] and Hf-based[27] systems. Several successful compositions were designed using P_{HS} and P_{HSS} parameters.[28] The current research focuses on exploring the thermodynamic and topological parameters like ΔH_{chem}, $\Delta S_\sigma/k_B$ and $\Delta S_c/R$ on the glass formation in the Zr–Cu–Al–Ag system.

Zr-based BMGs are of immense interest due to their exceptional GFA and characteristic properties like excellent mechanical strength, good corrosion-resistant and low Young's modulus(~ 80 GPA).[28,29] Zr-based ternary alloys with critical diameters of more than 10 mm were reported earlier.[30,31] The critical diameter (d_c) is the largest possible specimen size that can be cast with a fully amorphous structure. The addition of various alloying elements like Al, Ni, Co, and Ag are used to improve the physical, chemical and mechanical properties of Zr-containing alloys.[32] Zr–Cu binary alloy exhibited a full glassy structure having a d_c of 2 mm for the $Cu_{64.5}Zr_{35.5}$ composition.[33] The incorporation of specific elements leads to a reduction in the liquidus temperature, consequently enhancing GFA.[34,35] The addition of Al in the Zr–Cu system leads to an increase in its d_c to 5 mm for $Zr_{48}Cu_{45}Al_7$composition.[36] Similarly, Ag addition exceptionally improves the GFA and thermal stability of the Zr–Cu glass-forming system.[37] Ag addition also enhances the tensile plasticity making BMGs suitable for load bearing bio implant applications. It is reported that $Zr_{45}Cu_{45}Ag_{10}$ has a d_c of 6.0 mm and shows high-fracture strength and a notable plastic strain (0.2 pct).[38] d_c value of 25 mm is reported for the $Zr_{48}Cu_{36}Al_8Ag_8$

BMG with good plasticity and excellent fracture strength of 1850 MPa.[39] Prior to this work, the influence of adding Ag to the Zr–Cu system has been extensively studied by various researchers.[40–42] These studies have revealed that the introduction of Ag significantly enhances the GFA of Zr–Cu–Al–Ag metallic glass systems. In the present work, efforts have been made to narrow down the specific GFA regions based on the amount of Ag addition.

Therefore, the motivation of the present study emphasizes on the need for a more comprehensive and reliable approach to predict the glass formation in metallic systems. In this present study, a quaternary composition was purposefully chosen, incorporating all four elements (Zr, Cu, Al, Ag) with careful attention given to their thermodynamic and topological aspects. While empirical rules and parameters,[16,17] have provided valuable guidelines, further research is required to refine and expand these principles for various alloy systems. In this study, the P_{HSS} parameter was introduced, which combines thermodynamic and topological factors to predict glass formation in the Zr–Cu–Al–Ag system. Also, it efficiently aids in identifying GFCs with high GFA. The study aims to develop an easier and more precise computational method to predict the GFCs without doing actual experiments. This approach will contribute to a more comprehensive understanding of BMGs formation and potentially lead to the development of advanced metallic glasses with improved GFA.

II. MATERIALS AND METHODS

The $Zr_{47}Cu_{40}Al_8Ag_5$ alloy was fabricated in the form of a 3 mm diameter rod using the copper mould suction casting process. The metals were melted using arc melting, and the resulting molten alloy was drawn into a rod shape using suction. Chemical homogeneity was ensured by melting the base materials multiple times. High purity metals with a purity of 99 pct for Zirconium (Zr), 99.9 pct for Copper (Cu), 99.8 pct for Aluminium (Al), and 99.9 pct for Silver (Ag) were used in the preparation of the alloy. X-ray diffraction (XRD) studies were used to investigate the crystallographic nature of the fabricated rod. This study was conducted using a Rigaku Smart lab X-ray diffractometer with a Cu-Kα source of wavelength 1.54 Å with a scanning rate of 2 deg/min. Transmission Electron Microscopy (TEM) studies were carried out by Jeol JEM 2100LaB6 version at 200 kV.

III. THERMODYNAMIC CALCULATIONS

A combination of two thermodynamic parameters, namely the enthalpy of chemical mixing (ΔH_{chem}) and the configurational entropy ($\Delta S_c/R$), along with a single topological parameter, the normalized mismatch entropy ($\Delta S_\sigma/k_B$), have been established to enable the identification of BMG compositions that exhibit improved GFA.

A. *Enthalpy of Chemical Mixing*

The enthalpy of chemical mixing was calculated based on an extended regular solution model for ternary systems proposed by Gallegos's approach.[43]

$$\Delta H_{chem} = \sum_{\substack{i=1 \\ i \neq j}}^{n} \Delta H_{ij}^{C} \quad [1]$$

Here,

$$\Delta H_{AB}^{C} = X_A X_B \left(X_B \Delta H_{A-B}^{interface} + X_A \Delta H_{B-A}^{interface} \right) \quad [2]$$

The enthalpy value as a result of mixing $\Delta H_{B-A}^{interface}$ is calculated from Miedema's semi-empirical model.[44]

B. *Mismatch Entropy*

Mismatch Entropy emerges due to the atomic size difference of constituent elements. $\Delta S_\sigma/k_B$ provides the compositional trend based on topological instability.[45] The impact of atomic size mismatch within a given system was evaluated using an empirical formula presented by Mansoori *et al.*[46]

$$\Delta S_\sigma = k_B \left[\frac{3}{2}(\zeta^2 - 1) y_1 + \frac{3}{2}(\zeta - 1)^2 y_2 - \left\{ \frac{1}{2}(\zeta - 1)(\zeta - 3) + \ln \zeta \right\} (1 - y_3) \right] \quad [3]$$

Here,

$$y_1 = \frac{1}{\sigma_3} \sum_{j \geq i=1}^{n} \left(d_i + d_j \right) \left(d_i - d_j \right)^2 C_i C_j \quad [4]$$

$$y_2 = \frac{\sigma_2}{(\sigma_3)} \sum_{j \geq i=1}^{n} \left(d_i d_j \left(d_i - d_j \right)^2 C_i C_j \right. \quad [5]$$

$$y_3 = \frac{(\sigma_2)^2}{(\sigma_3)^2} \quad [6]$$

$$\sigma_k = \sum_{i=1}^{n} C_i d_i^k, \; k = 2, 3, \quad [7]$$

where d_i and d_j are diameters of ith and jth element, whereas C_i and C_j are the concentration in at. pct. ξ is the packing fraction for dense random packing and is taken as 0.64 for the present study.[46] The value of ξ was determined through both experimental[46] and statistical methods,[47] yielding a consistent result of 0.64. The evaluation of ξ involved conducting experiments and applying statistical analyses, both of which independently led to the same value of 0.64. This convergence strengthens the reliability and confidence in terms of random packing by taking the value of 0.64 for ξ in presently studied Zr-based system.

C. *Configurational Entropy*

$$\Delta S_c = -R\sum_{i=1}^{n} x_i \ln x_i, \qquad [8]$$

where x_i is the atomic percentage of the ith element and R is the Universal gas constant.

IV. RESULTS AND DISCUSSION

In the present study, thermodynamic modelling is used to optimize the composition in the Zr–Cu–Al–Ag quaternary system. The system is sub-divided into four possible ternary systems, Zr–Cu–Al, Zr–Cu–Ag, Zr–Al–Ag and Cu–Al–Ag. To predict the composition in the Zr–Cu–Al–Ag system, the most negative P_{HS} value is taken into consideration for Zr-rich containing ternary systems and the least negative P_{HS} value is chosen for non-Zr ternary systems considering the amorphous phase stability in Zr-based systems. As mentioned earlier that theP_{HS}, is the product of the enthalpy of chemical mixing and mismatched entropy normalized by the Boltzmann constant, represents the bonding energy associated with a system. In this context, a negative P_{HS} value indicates the energy required for a system to achieve stability, as stable systems tend to have the minimum energy state. Conversely, positive P_{HS} values do not meet the criterion of minimum energy and suggest lack of stability. Hence, to ensure the stability of Zr-based systems, the most negative P_{HS} value is selected, as it represents the minimum energy state for such compositions. On the other hand, non-Zr-based systems may have positive P_{HS} values, indicating higher energy levels and potential instability when compared to Zr-based systems. By considering the most negative P_{HS} for Zr-based systems and the relative values for non-Zr-based systems, the stability and energy minimization for Zr-based compositions is prioritized in the study.

The weighted approach uses P_{HS} values determined from the ternary system to design the quaternary composition.[48] The weighted average is a mathematical approach to find the quaternary composition from sub-ternaries by taking into account of phase stability in the amorphous structure for the ternary system using the P_{HS} values.The averaging is performed based on the following formula.

$$C_i = \sum_j C_i^j \times \frac{P_{HS}^j}{(P_{HS})_T},$$

where

$$(P_{HS})_T = \sum_j P_{HS}^j$$

Here C_i is the desired composition of ith element, $P^j{}_{HS}$ is the P_{HS} value of the jth ternary system and $(P_{HS})_T$ is the sum of all P_{HS} values of ternary systems.

For each ternary system, the optimized compositions from the ternary diagram were obtained using thermodynamic parameters; ΔH_{chem}, $\Delta S_c/R$ and topological parameter $\Delta S_\sigma/k_B$. ΔH_{chem} gives an indication of the phase stability of the alloy system.[49] Lower enthalpy values results in cluster formation that destabilizes the crystalline structure and makes glass formation easier.[49] By varying the enthalpy values in small intervals, we get contours of ΔH_{chem} for a ternary system. Similarly, iso-contours are also plotted for $\Delta S_\sigma/k_B$ which mainly depends on the atomic diameters of the constituent elements present in system.[50] The third thermodynamic parameter, *i.e.,* $\Delta S_c/R$ does not depend upon the element's physical or chemical characteristics and is solely dependent on the configuration chosen by atoms using Stirling's approximation.[51] For a multi-component system, configurational entropy has a significant impact on glass formation as it guides how the different atomic clusters settle themselves to restrict long-range order.[52] The larger value of configurational entropy ensures stability in metallic glasses.[52] Various studies have shown that for the ternary systems, the GFCs tend to fall within a specific range of configurational entropy, typically between 0.9 and 1.0.[53,54] Hence, the range of 0.9-1.0 is considered in the current work. In Figure 1, the atom configurations are depicted, illustrating the importance of configurational entropy values. These values are determined by employing the configurational entropy formula and leveraging the principles of permutation and combination.

Isometric contours of ΔH_{chem}, $\Delta S_\sigma/k_B$ and $\Delta S_c/R$ are drawn for all the four sub ternary systems. Figures 2 and 3 represent the plots of this graphical approach where the ΔH_{chem} and S_σ/k_B isometric contours are drawn for sub ternary systems of the Zr–Cu–Al–Ag system. Each contour line represents a particular value of the thermodynamic and topological parameters taken into consideration.

Figure 2(a) demonstrates the isometric ΔH_{chem} contours for the Cu–Al–Ag ternary system, where the negative enthalpy is − 21 kJ/mol at the Zr–Cu end. As we move towards the Zr–Ag end, enthalpy increases. These phenomena result from differences in the values of enthalpy between various binary systems. Values of ΔH_{chem} among binary pairs taken from enthalpy at infinite dissolution is extensively calculated in Miedema's work.[41] The values of enthalpy are, $\Delta H_{Zr\ in\ Cu}$ = − 110 kJ/mol, $\Delta H_{Cu\ in\ Zr}$ = − 78 kJ/mol, $\Delta H_{Ag\ in\ Cu}$ = 10 kJ/mol, $\Delta H_{Cu\ in\ Ag}$ = 8 kJ/mol, ΔH_{AginZr} = − 78 kJ/mol and $\Delta H_{Zr\ in\ Ag}$ = 87 kJ/mol.[41] The negative values of enthalpy among the constituent elements ensure the stability of the glassy phase due to the higher chemical interaction among them resulting in a stronger metallic bond between the constituent elements.[55] It is necessary to obstruct the nucleation of the crystalline phase for glass formation.[56] Multiple phases exist at the lower enthalpy values during the solidification, leading to the formation of several distinct clusters like octahedron and icosahedral, which promotes easy glass formation due to the long-range order frustration in the alloy during solidification.[57]

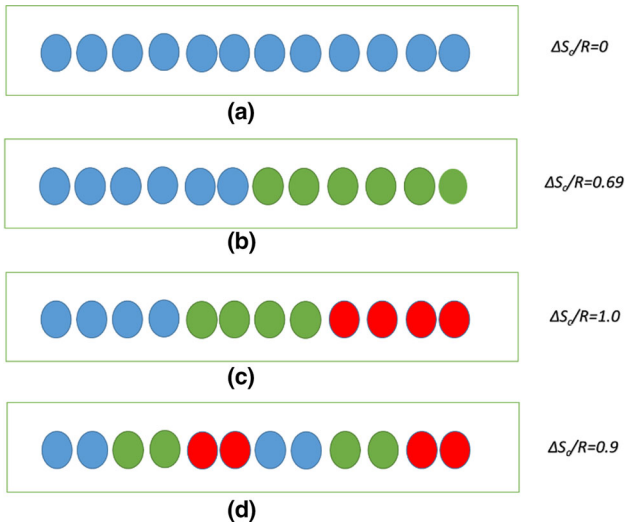

Fig. 1—Representation of different configurational values in crystalline, binary and ternary systems.

Figure 2(b) depicts the $\Delta S_\sigma/k_B$ isometric contours of the Cu–Zr–Ag system. The extreme mismatch entropy of 0.25 is detected at the Zr–Cu binary side, and it reduces as we move towards the Zr–Ag side in ternary phase diagram. Mismatch entropy quantifies disorder created by the constituent atoms due to their difference in atomic diameters.[58] So, the larger the mismatch entropy, the higher the disorder and, hence, the glass formation will be more accessible.[59] For the larger mismatch entropy, the atomic size difference should be large enough to destabilise the periodic arrangements among atoms.[59] The covalent diameters of Zr, Cu, Al and Ag are 2.9 Å, 2.34 Å, 2.5Åand 2.68 Å, respectively.[60] It can be observed that there is little difference in atomic size between Cu and Ag, in contrast, there is a larger difference in the case of Zr and Cu. Thus, a larger mismatch entropy is evident on the Zr–Cu side of the ternary diagram. Figure 2(c) represents the iso-contours of $\Delta S_c/R$. The inner contour represents the value of 1.0, and the outer contour shows the value of 0.9.

The superimposition of all the isometric contours is shown in Figure 2(d). The combination of the lowest enthalpy and larger mismatch entropy plays an important role in glass formation since it destabilizes crystalline systems to induce dense random packing with irregular atomic arrangement. Hence, intersection points of isometric contours of $\Delta S_\sigma/k_B$ and ΔH_{chem} in the $\Delta S_c/R$ range of 1.0 to 0.9 are the regions of interest from thermodynamical and topological aspects.

P_{HS} value is calculated at each intersection point within the 0.9-1.0 range of $\Delta S_c/R$, as shown in Table I. Similarly, superimposed contours are plotted for the other three sub ternary systems (Zr–Al–Ag, Zr–Cu–Al and Cu–Al–Ag) and the P_{HS} values are determined at the intersection points. Figure 3 shows the iso-contours for the (a) Zr–Al–Ag, (b) Zr–Cu–Al and (c) Cu–Al–Ag sub ternary systems. Table I shows the compositions of all the intersection points with their P_{HS} values in brackets. For Zr-based systems, the composition with the most negative P_{HS} is selected, while for non-Zr-based systems like Cu–Al–Ag, the composition with the most positive P_{HS} is chosen to ensure the stability of the system. The weighted average is taken on the selected compositions to design the quaternary compositions tabulated in Table II.

The composition obtained from the above modelling approach is $Zr_{44}Cu_{32}Al_{18}Ag_6$. It was observed that the obtained composition does not lie in the vicinity of reported compositions.[61] This technique was successfully utilized earlier to optimize the good GFC in ternary,[62] quaternary[63] and quinary systems.[64] The modelling was highly successful on many systems but due to the selection of elements like Al and Ag for this particular system, the earlier method does not identify GFC in Zr–Cu–Al–Ag system using the graphical approach. Also, variation in modelled and reported compositions is due to the error in selecting the intersection points when using this graphical method. In this approach, the range and intervals of thermodynamic parameters (ΔH_{chem}, $\Delta S_\sigma/k_B$, and $\Delta S_c/R$) are selected in optimum range so that the contours should not overlap with each other. This leads to the underestimation of some values in between the iso-contours lines. Therefore, it becomes difficult to obtain all intersection points within the range of $\Delta S_c/R$ using a graphical approach.

This fetched the motivation for the present work wherein a new and fast computational approach, where all the possible points can be obtained within the $\Delta S_c/R$ range. Our modeling results directly gave the P_{HS} points with most negative values in the $\Delta S_c/R$ range. The flow chart used to implement the program is shown in Figure 4.The flowchart presented in Figure 4 employs symbols A, B, and C, representing the ternary system A–B–C. These symbols correspond to the respective elements. The incremental value denotes the amount by which the atomic percentage increases for a specific element. If the incremental value is small, the program's runtime will be extensive. Conversely, if the incremental value is too high, there is a possibility of missing out on more values. Therefore, based on the understanding gained from the previous graphical method, an incremental value of 0.2 is chosen for elements A and B.

The weighted average is taken to design the quaternary system from the P_{HS} of ternary systems obtained using the computational approach shown in Table III. The composition obtained from the computational approach is $Zr_{47}Cu_{40}Al_8Ag_5$ with a P_{HSS} value of − 4.64 kJ/mol and lies in the close vicinity of reported compositions.[65] The P_{HSS} method has been widely adopted by researchers to accurately predict the GFA of BMGs and both P_{HSS} and P_{HS} are considered as critical GFA parameters. Yuan *et al.*[66] have also explored the P_{HSS} method and demonstrated its effectiveness for the Zr–Cu–Al–Ag system. By employing iso-P_{HSS} contours, it has been shown that the P_{HSS} parameter can offer valuable insights into a range of BMG compositions that exhibit a high GFA. Furthermore, other researchers have explored the application of machine learning methods to better understand the P_{HSS} parameters affecting the GFA.[67,68] The P_{HSS} method has been successfully utilized by earlier results and is widely

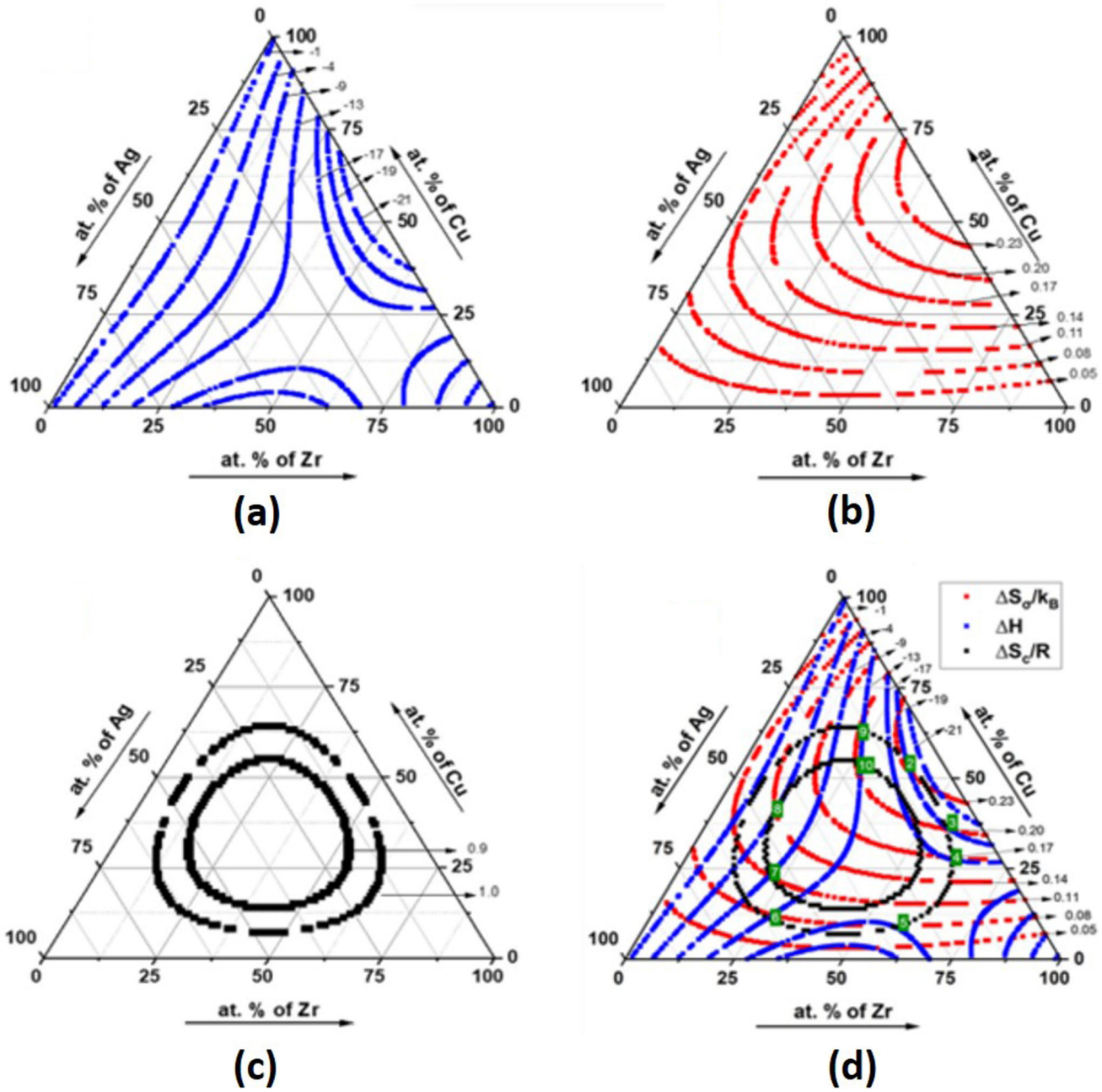

Fig. 2—Isometric contours of (*a*) ΔH_{chem} for Zr–Cu–Ag system (*b*) $\Delta S_{\sigma}/k_B$ for Zr–Cu–Ag system (*c*) $\Delta S_c/R$ for Zr–Cu–Ag system (*d*) Superimposition of ΔH_{chem}, $\Delta S_{\sigma}/k_B$, and $\Delta S_c/R$ for Zr–Cu–Ag system.

accepted for Zr-based systems.[69,70] Additionally, it has also been applied to some Ca-based[71] and Fe-based systems.[72] As a GFA parameter, P_{HSS} exhibits a strong correlation with GFA, where a more negative P_{HSS} value indicates a higher possibility of glass formation.[73] The P_{HSS} method is based on Inoue's three empirical rules, which are generally followed by most systems regarding glass formation, although exceptions do exist. While we cannot claim that the P_{HSS} method is a universally applicable approach for determining BMG compositions, it has been extensively proven and accepted for Zr-based systems. This method derives a final composition based on the most negative P_{HSS} value. However, it is important to note that there can be multiple compositions that exist within the same P_{HSS} region, and alternative compositions can also be obtained.

The X-ray diffraction (XRD) spectra of the top and bottom of $Zr_{47}Cu_{40}Al_8Ag_5$ BMG rod are shown in Figure 5(a). The broad and diffused halo peak in the spectrum is a sign of an amorphous phase. Notably, the lack of any distinct Bragg peaks in the spectra suggests that the BMG structure lacks long-range atomic ordering or crystalline phase. Thus, the XRD results confirm the amorphous nature of the modelled $Zr_{47}Cu_{40}Al_8Ag_5$ BMG rod. The HRTEM image unveils a maze-like

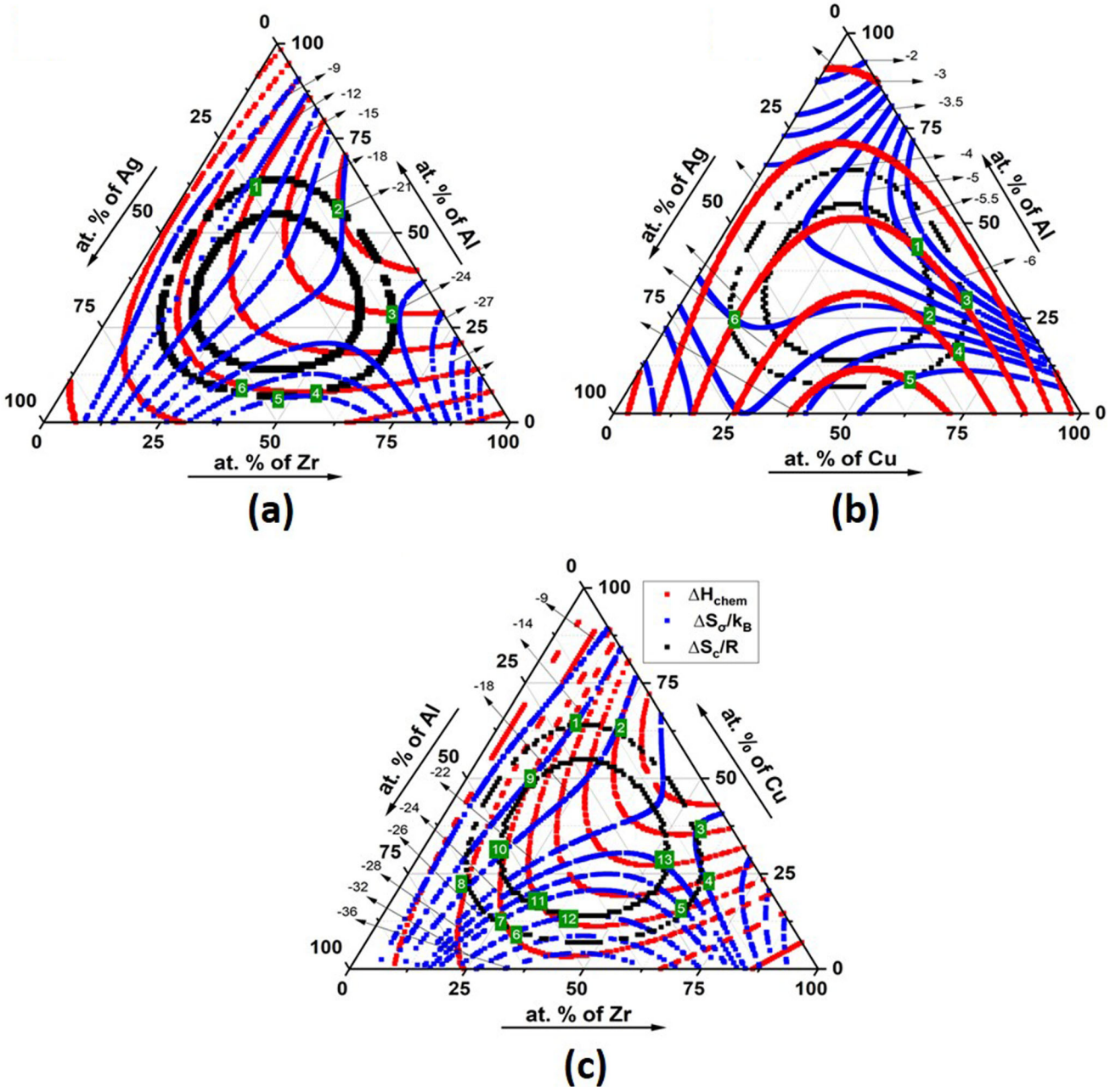

Fig. 3—Superimposition of ΔH_{chem}, $\Delta S_{\sigma}/k_B$, and $\Delta S_c/R$ for (*a*) Zr–Al–Ag, (*b*) Zr–Cu–Al and (*c*) Cu–Al–Ag systems.

contrast characterized by the absence of clear lattice fringes, demonstrating the amorphous nature of the alloy. The selected area electron diffraction (SAED) pattern, shown in the inset additionally supports the glassy nature of the metallic glass (MG). The presence of halo diffuse rings without distinct diffraction spots in the SAED pattern shows the lack of long-range order, confirming the amorphous structure. The primary aim of our study was to predict GFCs using thermodynamic modelling and then verify those predictions through experimentation. We carried out XRD and TEM investigations to confirm the nature of the $Zr_{47}Cu_{40}Al_8Ag_5$, alloy. From the XRD and TEM analysis, it has been found out that the alloy is amorphous in nature which validates our present model. The results of our successful experimental validation using suction casting confirm that our predictions are accurate. The finding also indicates that other pseudo-ternary glasses (Zr–Cu–Al, Zr–Cu–Ag) formed in the system also confirm the validity of the present model.

Table IV [74,75] shows the reported compositions and their change in the atomic pct of the constituent elements with respect to the modelled composition. Figure 6(a) is a graphical representation of the same. It is evident from the table that a significantly small compositional change affects the GFA considerably. It is observed that the variation in Zr and Al is significantly low in comparison to Cu and Ag. It is evident

from the table that a small variation in the atomic pct has a significant effect on d_c. Hence, it is crucial to carefully control the compositions of Cu and Ag to obtain a good GFA composition. The graph also shows that the composition obtained using the graphical approach ($Zr_{44}Cu_{32}Al_{18}Ag_6$) does not lie in the glass-forming region depicted by the reported compositions. It is shown in figure 6(a) that the particular element's atomic pctcan vary in a certain band but in the graphical approach, Al and Cu present in the composition ($Zr_{44}Cu_{32}Al_{18}Ag_6$)), lies far from the band. So, the current method is justified using computational techniques. The difference in atomic size between Ag and Al is only 1.03 pct, which is less than 12 pct and there is a positive enthalpy of mixing between Ag and Cu, *i.e.*, $\Delta H_{Ag\ in\ Cu} = +10$ k J/mol. The current Zr–Cu–Al–Ag system deviates from two rules proposed by Inoue therefore, it results due to an insignificant difference from the reported composition. Earlier metallic glass composition optimization approaches were only based on trial-and-error methods.[76] However, thermodynamical and topological modelling gives a more logical approach in pinpointing GFC.

The P_{HSS} calculation was done for all the reported compositions shown in Table IV. Since P_{HSS} is used to determine the GFC and most negative P_{HSS} signifies the best GFC, no correlation is shown by the reported composition as most negative P_{HSS} does not result in larger d_c. Although the composition with the most negative P_{HSS} in the system does not correspond to the best GFC, P_{HSS} gives an idea about the potential region in which the largest d_c composition can be obtained. It is observed that most of the reported compositions adhere around a particular P_{HSS} region. Hence, there could be a range of P_{HSS} values to find good GFCs.

The P_{HSS} is an excellent parameter to find the GFC because it takes account of all the considered parameters, *i.e.*, ΔH_{chem}, $\Delta S_\sigma/k_B$ and $\Delta S_c/R$. Figure 6(b) is showing the variation of P_{HSS} with respect to the critical diameter (d_c).The graph shows the R^2 value of 60 pct, which is good fit on the P_{HSS} approach. Here R^2 is the linear correlation coefficient. When there is a significant difference in atomic size between two elements, the smaller atoms can occupy interstitial positions within the lattice with minimal strain, leading to the formation of compounds that possess a favourable crystal structure..[77] Also, more negative enthalpy of mixing leads to the compound formation and positive enthalpy leads to segregation of atoms.[77] The configurational entropy decides the randomness in the system and allows the atoms to position themselves in the most probable arrangement. Hence, considering only the parameter that makes it difficult to determine glass-forming composition; and intermediate values of ΔH_{chem} and $\Delta S_\sigma/k_B$ have been taken to model the GFC. Denser random packing leads to difficulty in atomic rearrangements and large liquid/solid interfacial energy is achieved resulting in low atomic diffusivity and high viscosity. This enables the easy glass formation.[73]

Figure 6(c) represents the plot between ΔT_x and d_c of reported compositions from literature. ΔT_x indicates the quantitative values for the SCLR. The plot shows the R^2 value of 53 pct which is less than the R^2 value of d_c *vs* P_{HSS}. This again suggests that P_{HSS} is a more reliable parameter in comparison to ΔT_x since the ΔT_x criteria are based on the SCLR stability. The ΔT_x parameter only speculates about the stability of the SCLR without providing any evidence about the glass formation kinetics.[73] The large liquid-solidus interfacial energy results in high GFA that arises from the atomic bonding and their packing positions, attributed to the high negative ΔH_{chem} and large atomic size ratios.[78] On the contrary, P_{HSS} utilises the thermodynamical and topological aspects of the glass-forming system. One of the prime advantages of P_{HSS} is that it is a theoretical parameter that allows us to predict the GFA of a composition before the composition is synthesised.

Earlier P_{HS} and P_{HSS} were used for ternary and higher-order systems, respectively. To understand the influence of each element, an attempt has been made to determine the thermodynamic nature using P_{HS} and P_{HSS} in binary systems. Considering the miscibility between the elements, the present alloy system can be divided into two dominant species, one is Zr-rich and another is Cu-rich. To understand the role of each species pseudo-binary diagrams are developed by taking Zr on the one side and the rest of the elements on the other side. Figure S1 (Supplementary file) represents ΔH_{chem}, $\Delta S_\sigma/k_B$, $\Delta S_c/R$, P_{HS} and P_{HSS} contours for each sub-binaries of the Cu–Zr–Al–Ag quaternary system. The sub-binaries are (a) Zr–Cu (b) Cu–Al (c) Al–Ag (d) Cu–Ag (e) Zr–Al and (f) Ag–Zr. We can consider these diagrams as Zr–Cu (Al, Ag) pseudo-binary. The extreme values of P_{HS}, P_{HSS}, ΔH_{chem}, $\Delta S_\sigma/k_B$ and $\Delta S_c/R$ with their respective compositions are shown in Table V.

The configurational entropy and mixing enthalpy decide the stability of the specific phase in the particular binary diagram. There is a similarity in Figures S1(a), (e), and (f) as discussed above in the pseudo-binary approach. A difference is observed between P_{HS} and P_{HSS} values for each binary system since P_{HSS} incorporates the value of configurational entropy. The same value of configurational entropy is obtained for all the binary systems as it is based on the position of the respective atoms. However, P_{HS} is less than the P_{HSS} value except for the Cu–Ag system owing to its positive enthalpy of mixing. The lower value of P_{HS} is justified because when there are only two types of species present in a system, only one configuration possible. When there is a ternary or higher-order system many configurational structures possible based on the Stirling approximation. Hence, configuration entropy is not playing a significant role in deciding the randomness in binary systems. Zr–Cu is an excellent binary glass former due to its most negative P_{HS} and P_{HSS} among all the binary curves. Zr–Al has the most negative mixing enthalpy compared to Zr–Cu, still it does not facilitate glass formation due to the low mismatch entropy value. It was proposed by Egami and Waseda[79] that the minimum solute concentration needed for the glass formation in binary alloys is inversely proportional to atomic size mismatch. Hence, the solid solution configuration should be suppressed for facilitating the glass formation. This requires a large atomic size difference and negative enthalpy of mixing.

Table I. Ternary Compositions with P_{HS} (kJ/mol) Values

Zr–Cu–Al(P_{HS})	Zr–Cu–Ag(P_{HS})	Zr–Al–Ag(P_{HS})	Cu–Al–Ag(P_{HS})
$Zr_{15.2}Cu_{63.56}Al_{21.3}$(− 3.09)	$Zr_{22.3}Cu_{64.1}Ag_{13.6}$(− 2.75)	$Zr_{13.2}Al_{62.8}Ag_{24}$(− 1.35)	$Cu_{41.6}Al_{44.4}Ag_{14}$(− 0.27)
$Zr_{25.7}Cu_{62.6}Al_{11.7}$(− 4.29)	**$Zr_{37}Cu_{54.4}Ag_{8.6}$(− 4.40)**	**$Zr_{35.2}Al_{56.5}Ag_{8.3}$(− 3.90)**	$Cu_{54.7}Al_{23}Ag_{20.3}$(− 0.05)
$Zr_{56.2}Cu_{35.4}Al_{8.4}$(− 4.44)	$Zr_{55}Cu_{36.7}Ag_{8.3}$(− 3.8)	$Zr_{61.3}Al_{29.1}Ag_{9.6}$(− 2.70)	$Cu_{60.8}Al_{29.5}Ag_{9.7}$(− 0.16)
$Zr_{63.7}Cu_{23.5}Al_{12.8}$(− 3.24)	$Zr_{61.3}Cu_{27.7}Ag_{11}$(− 2.79)	$Zr_{55}Al_{7.5}Ag_{37.5}$(− 0.43)	$Cu_{64.2}Al_{16.8}Ag_{19}$(− 0.05)
$Zr_{64.3}$ $Cu_{15.7}Al_{20}$(− 2.56)	$Zr_{57.6}Cu_{9.4}Ag_{33}$(− 0.95)	$Zr_{46}Al_{7}Ag_{47}$(− 0.37)	**$Cu_{58.3}Al_{9}Ag_{32.7}$(0.003)**
$Zr_{30}Cu_{9.6}Al_{60.4}$(− 1.83)	$Zr_{27}Cu_{12.3}Ag_{60.7}$(− 0.82)	$Zr_{38.1}Al_{8.7}Ag_{53.2}$(− 0.43)	$Cu_{13.1}Al_{24.6}Ag_{62.3}$(− 0.16)
$Zr_{26.3}Cu_{13.0}Al_{60.7}$(− 2.27)	$Zr_{21.6}Cu_{23.4}Ag_{55}$(− 1.02)		
$Zr_{14.6}Cu_{22}Al_{63.4}$(− 2.43)	$Zr_{14.2}Cu_{40.7}Ag_{45.1}$(− 0.82)		
$Zr_{13.3}Cu_{48.7}Al_{38}$(− 3.08)	$Zr_{22}Cu_{64.4}Ag_{13.6}$(− 2.71)		
$Zr_{17.3}Cu_{30.7}Al_{52}$(− 3.12)	$Zr_{26.5}Cu_{54.2}Ag_{19.3}$(− 2.72)		
$Zr_{38.9}Cu_{13.8}Al_{47.3}$(− 3.00)			
$Zr_{54.1}Cu_{27.7}Al_{18.2}$(− 2.69)			

The most negative PHS value from the Zr-based system and the most positive value from non-Zr-based system are highlighted in bold

Table II. Alloy Design by Weighing Approach Using P_{HS} Values from Figs. 1 and 2

Composition	P_{HS} (kJ/mol)
$Zr_{56.2}Cu_{35.4}Al_{8.4}$	− 4.44
$Zr_{37}Cu_{54.4}Ag_{8.6}$	− 4.40
$Zr_{35.2}Al_{56.5}Ag_{8.3}$	− 3.90
$Cu_{58.3}Al_{9}Ag_{32.7}$	0.003
$Zr_{44}Cu_{32}Al_{18}Ag_{6}$ (Modelled by Graphical Approach)	− 3.91

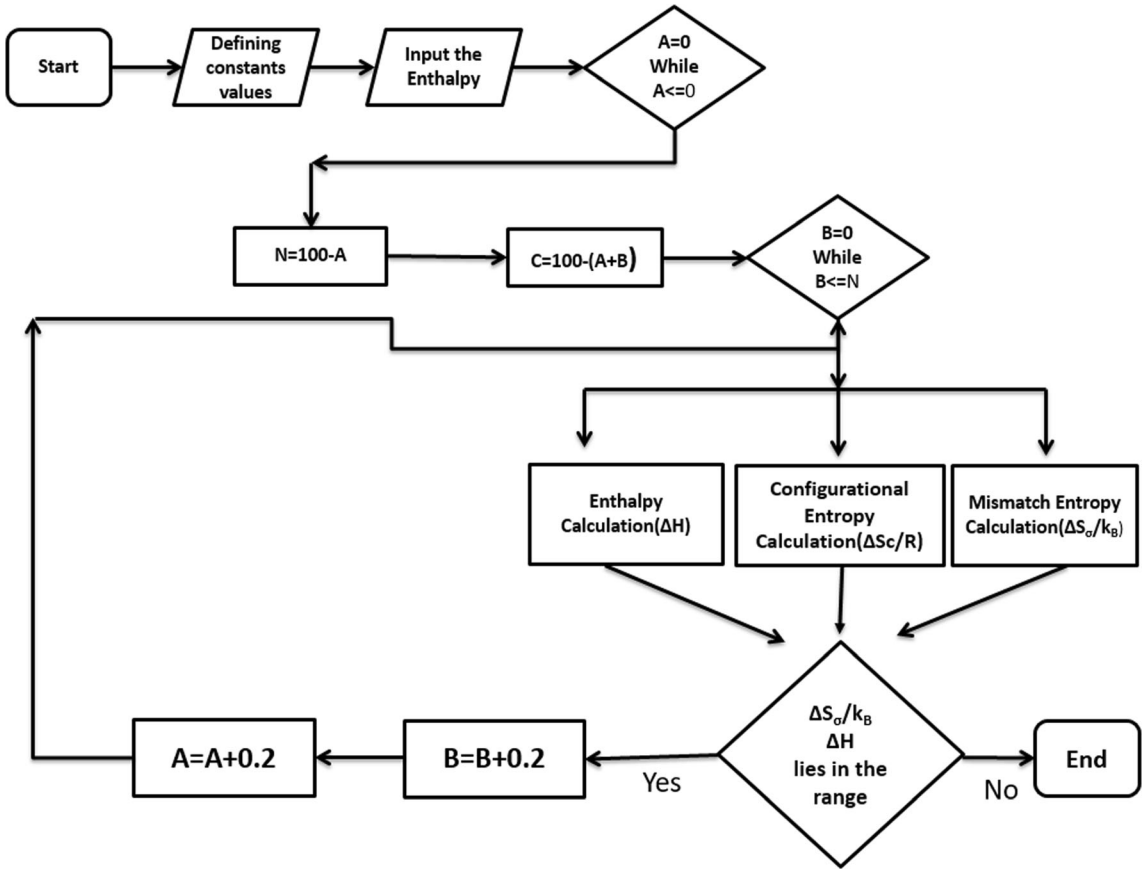

Fig. 4—Flow chart of the program calculating the P_{HSS}.

Table III. Alloy Design by Weighing Approach Using P_{HS} Values from Coding

Composition	P_{HS} (kJ/mol)
$Zr_{42.4}Cu_{50.2}Al_{7.4}$	− 5.34
$Zr_{42.7}Cu_{50}Ag_{7.3}$	− 4.65
$Zr_{60.9}Al_{27.5}Ag_{11.6}$	− 2.44
$Cu_{37}Al_{8.1}Ag_{54.9}$	0.013
$Zr_{47}Cu_{40}Al_8Ag_5$ (Modelled by Coding Approach)	− 4.32

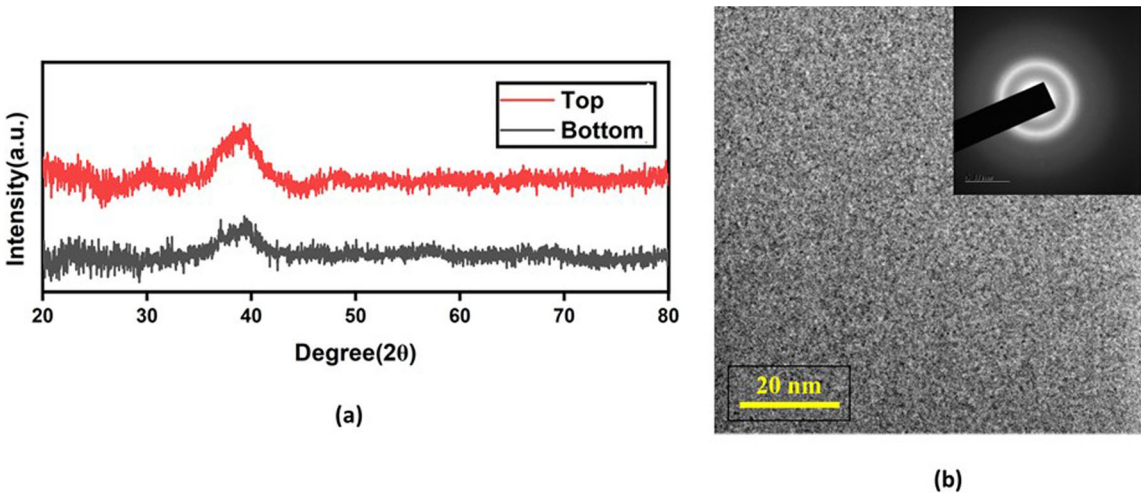

Fig. 5—(*a*) XRD graph (*b*) Bright field HRTEM image with SAED pattern of modelled BMG composition $Zr_{47}Cu_{40}Al_8Ag_5$.

As reported in the literature, the binary glass of the Zr–Cu system is produced within a 2 mm diameter.[80] However, the addition of alloying elements increases the GFA of metallic glasses. The addition of Al increases the GFA of the Zr–Cu system up to 6 mm in diameter.[81] The enthalpy of Zr–Al is – 44 kJ/mol, which is very large as compared to Zr–Cu enthalpy, which is – 23 kJ/mol. Hence the Al addition is only limited to the 10 at. pct and further addition of Al leads to the formation of the intermetallic, reducing the GFA.[66] The addition of the fourth element, Ag, improves the GFA without forming the intermetallic compound. Ag is chosen due to its negative enthalpy of mixing with Zr and Al. Also, due to its significant difference in atomic diameter with respect to Zr and Cu, the mismatch entropy of the system is increased. The enthalpy of Zr–Ag is –20 kJ/mol, which is near to Zr–Cu (− 23 kJ/mol) therefore replacing Cu with Ag in this system facilitates the formation of a glassy phase. It was reported that the Cu-centered Cu_6Zr_7 and Cu_8Zr_5 icosahedral clusters are the primary polyhedral clusters in Zr–Cu metallic glasses.[82] It was observed that the minor addition alloying elements in Zr-based metallic glass showed no change in coordination number. (CN) of the clusters.[83] Therefore we can say that the minor addition of Ag does not change in CN number due to mutual repelling of Cu and Ag articulated resulting from positive enthalpy of Cu–Ag (2.25 kJ/mol). Also, the enthalpy of mixing between Al–Ag is less negative (− 4 kJ/mol); therefore, Al and Ag addition is limited to a few atomic pct only.

It has always been a challenge to represent GFA parameters for quaternary systems. Further investigating the P_{HSS} applicability for the proposed Zr- based system, an attempt was made to represent the quaternary system by fixing the composition of Ag and taking the ternary graphs of the rest without normalising the composition to get a ternary diagram instead of a quaternary as shown in Figure S2(Supplementary file). The heat map represents the P_{HSS} of the corresponding compositions in the form of a ternary graph. To observe the effect of variation in atomic pct of Ag, all ternary graphs are stacked with increasing Ag at. pct in the range 1-8, as shown in Figure 7. The red line shows the most negative P_{HSS} line in the pseudo-quaternary graph. It was expected to have a uniform shift as we increased the Ag content, which is represented by connecting the most negative P_{HSS} composition in each ternary graph. Surprisingly, there was little variation from the trend at 4 to 5 at pct Ag. It is interesting to note that the present modelled composition has 5 at. pct Ag, which falls in this indefinite area of the quaternary plot. It is observed that as we increase at. pct of Ag till 4 pct, the composition replaces Ag with Al which has the highest negative P_{HSS}. But as we cross 5 at. pct Ag, further addition of Ag replaces Cu to obtain a higher negative P_{HSS} composition. It is important to note that this occurs at 7 at. pct Al, which is also the fixed at. pct of Al for most of the reported compositions which are observed in

Table IV. Percentage Atomic Difference in Elements of Modelled Composition with Respect to the Reported Compositions Along with Its Critical Diameter

S. No.	Compositions	Atomic Pct Difference (w. r. t. Modelled Composition)	ΔH (kJ/mol)	$\Delta S_\sigma / k_B$	$\Delta S_c / R$	P_{HSS} (kJ/mol)	ΔT_X (K)	d_c (mm)	References
1.	$Zr_{48}Cu_{43}Al_7Ag_2$	Zr = − 1 Cu = − 3 Al = 1 Ag = 3	− 21.41	0.22	1.05	− 4.75	61	12	[74]
2.	$Zr_{48}Cu_{40}Al_7Ag_5$	Zr = − 1 Cu = 0 Al = 1 Ag = 0	− 20.08	0.22	0.98	− 4.58	70	10	[74]
3.	$Zr_{48}Cu_{42}Al_7Ag_3$	Zr = − 1 Cu = − 2 Al = 1 Ag = 2	− 20.93	0.23	0.98	− 4.71	63	10	[74]
4.	$Zr_{43}Cu_{45}Al_7Ag_5$	Zr = 4 Cu = − 5 Al = 1 Ag = 0	− 19.84	0.23	1.06	− 4.70	67	6	[74]
5.	$Zr_{43}Cu_{47}Al_7Ag_3$	Zr = 4 Cu = − 7 Al = 1 Ag = 2	− 20.73	0.24	1.01	− 4.81	67	5	[74]
6.	$Zr_{43}Cu_{49}Al_7Ag_1$	Zr = 4 Cu = − 9 Al = 1Ag = 4	− 23.14	0.25	0.94	− 8.11	66	4	[74]
7.	$Zr_{45}Cu_{45}Al_5Ag_5$	Zr = 2 Cu = − 5 Al = 3 Ag = 0	− 20.16	0.24	1.02	− 4.64	86	9	[74]
8.	$Zr_{42}Cu_{42}Al_8Ag_8$	Zr = 5 Cu = − 2 Al = 0 Ag = − 3	− 18.49	0.22	1.13	− 4.48	75	12	[74]
9.	$Zr_{44}Cu_{40}Al_8Ag_8$	Zr = 3 Cu = 0 Al = 0 Ag = − 3	− 18.68	0.22	1.13	− 4.46	98	15	[74]
10.	$Zr_{45}Cu_{45}Al_3$ A_{g7}	Zr = 2 Cu = − 5 Al = 5 Ag = − 2	− 19.56	0.24	1.01	− 4.43	80	7	[74]
11.	$Zr_{45}Cu_{45}Al_7$ A_{g3}	Zr = 2 Cu = − 5 Al = 1 Ag = 2	− 20.86	0.24	1.01	− 4.80	78	8	[75]
12.	$Zr_{46}Cu_{46}Al_4Ag_4$	Zr = 1 Cu = − 6 Al = 4 Ag = 1	− 20.77	0.24	0.97	− 4.65	81	6	[75]
13.	$Zr_{44}Cu_{44}Al_6Ag_6$	Zr = 3 Cu = − 4 Al = 2 Ag = − 1	− 19.58	0.23	1.06	− 4.61	92	10	[75]
14.	$Zr_{46}Cu_{38}Al_8Ag_8$	Zr = 1 Cu = 2Al = 0 Ag = − 3	− 18.83	0.21	1.12	− 4.41	103	20	[75]
15.	$Zr_{50}Cu_{34}Al_8Ag_8$	Zr = − 3 Cu = 6 Al = 0 Ag = − 3	− 18.99	0.20	1.11	− 4.22	100	15	[75]
16.	$Zr_{48}Cu_{36}Al_8Ag_8$	Zr = − 1 Cu = 4 Al = 0 Ag = 3	− 18.93	0.21	1.12	− 4.33	108	25	[75]
17.	$Zr_{47}Cu_{40}Al_8Ag_5$ (modelled by computational approach)	—	− 20.02	0.21	1.06	− 4.64	—	—	

Figure 6(a).To further understand, the compositions from reported literature and their corresponding d_c are used in each ternary graph to connect and is represented by the blue line in the stacked quaternary graph. This blue line reflects our argument that the most negative P_{HSS} for a quaternary system does not directly correspond to the highest GFA composition. Although we can safely assume that the highest GFA composition of every Ag layer is not yet accurately identified from the available data. It is observed that there is a region surrounded by the blue line is in close vicinity with the reported compositions lie, and the modelled composition obtained using the current method lies in this region. This also gives us additional confirmation that the modelled composition has a good GFA.

From the above discussion, it can be said that the present work makes a significant intellectual contribution as it presents a novel computational method that revamps the finding of the glass-forming regions by simplifying the prediction of ternary GFCs. This method goes beyond ternary systems and can be used to model quaternary compositions as well. Moreover, the introduction of a pseudo-quaternary graph offers a crucial navigational tool to find precise regions favourable for glass formation. Hence, this novel approach opens up new possibilities for developing BMGs with better GFA.

V. CONCLUSIONS

This new computational approach is simple to use and provides accurate results thus, speeding up the process of finding the ternary GFCs. The ternary system predicted by this approach is used to model the quaternary composition $Zr_{47}Cu_{40}Al_8Ag_5$, which has a P_{HSS} value of − 4.87 kJ/mol. This value highlights the precision of the computational method by putting it close to compositions known for their significant GFA. A notable innovation in this paradigm is the use of a pseudo-quaternary graph, which is crucial in identifying a precise and refined portion of the P_{HSS} spectrum that is favourable to glass formation. This graph serves as a useful navigational aid by focusing on a narrowed-down glass-forming region within the overall compositional landscape. This focused identification greatly improves the research effectiveness and speeds up the prediction of GFCs. The understanding that even small changes in the atomic percentages of the constituent elements can produce a wide variety of compositions is an exciting aspect that results from the use of the P_{HSS} area. The sensitivity of GFA to such minute modifications highlights the complexity of ternary systems and further emphasises the reliability of the computational approach in revealing these complicated interactions. Overall, the accessibility, accuracy, and thorough insights provided by this computational technique bring up new possibilities for enhancing our comprehension and manipulation of ternary systems for improved glass-forming applications.

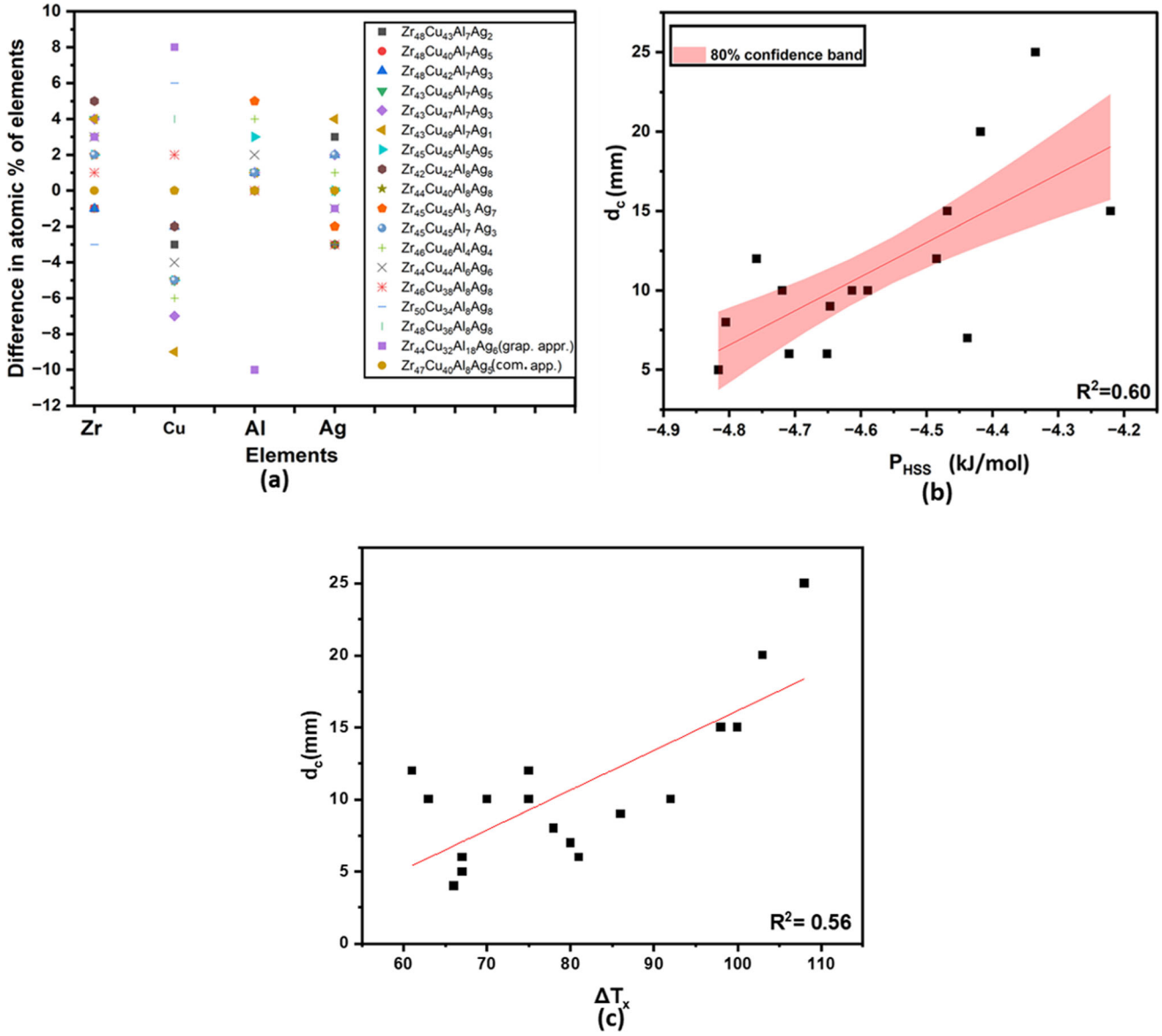

Fig. 6—(*a*) Difference in elemental compositions: modelled *vs* reported (*b*) Variation in P_{HSS} with respect to critical diameter (*c*) Variation of critical diameter (d_c) with ΔT_x.

Table V. P_{HS}, P_{HSS}, ΔH, $\Delta S_\sigma/k_B$ and $\Delta S_c/R$ Values from Binary Diagrams

System	P_{HS} (kJ/mol)	P_{HSS} (kJ/mol)	ΔH (kJ/mol)	$\Delta S_\sigma/k_B$	$\Delta S_c/R$
Zr–Cu	− 6.45($Zr_{44}Cu_{56}$)	− 4.42($Zr_{45}Cu_{55}$)	− 23.66($Zr_{46}Cu_{54}$)	0.27($Zr_{41}Cu_{59}$)	0.69($Zr_{50}Cu_{50}$)
Cu–Al	− 0.53($Cu_{53}Al_{47}$)	− 0.03($Cu_{52}Al_{48}$)	− 7.76($Cu_{52}Al_{48}$)	0.06($Cu_{54}Al_{46}$)	0.69($Cu_{50}Al_{50}$)
Al–Ag	− 0.002($Al_{50}Ag_{50}$)	− 0.001($Al_{50}Ag_{50}$)	− 4.37($Al_{51}Ag_{49}$)	0.0006($Zr_{50}Cu_{50}$)	0.69($Al_{50}Ag_{50}$)
Cu–Ag	0.18($Cu_{53}Ag_{47}$)	0.12($Cu_{53}Ag_{47}$)	2.25($Cu_{53}Ag_{47}$)	0.082($Cu_{55}Ag_{45}$)	0.69($Cu_{50}Ag_{50}$)
Ag–Zr	− 1.96($Ag_{53}Zr_{47}$)	− 0.82($Ag_{52}Zr_{48}$)	− 20.63($Ag_{51}Zr_{49}$)	0.058($Ag_{54}Zr_{46}$)	0.69($Ag_{50}Zr_{50}$)
Zr–Al	− 3.10($Zr_{47}Al_{53}$)	− 2.15($Zr_{48}Al_{52}$)	− 44.17($Zr_{48}Al_{52}$)	0.070($Zr_{46}Al_{54}$)	0.69($Zr_{50}Al_{50}$)

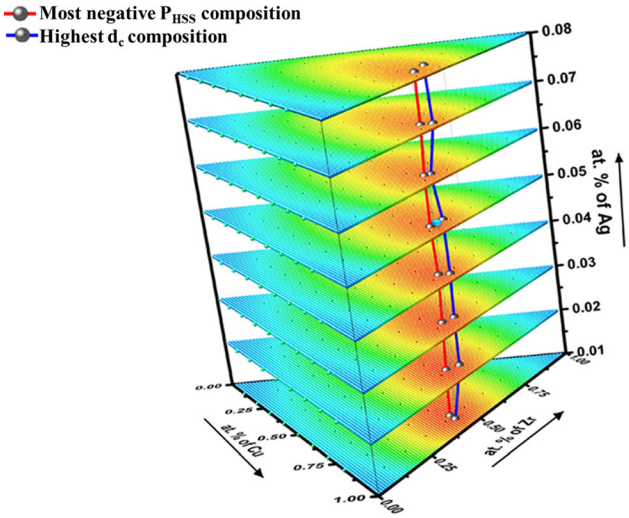

Fig. 7—Zr–Cu–Al–Ag BMG system with varying Ag atomic percentage.

ACKNOWLEDGMENTS

One of the authors (Jatin Bhatt) would like to acknowledge the CRG Project grant (CRG/2019/003674) funded by the Government of India for research support.

AUTHOR CONTRIBUTIONS

The authors are actively involved in Conceptualization- Jatin Bhatt, Juhi Verma Data curation- Juhi Verma, Sai Pranav Formal analysis-Juhi Verma, Sai Pranav, Abhilasha Jain, Jatin Bhatt Investigation- Juhi Verma, Sai Pranav Methodology- Juhi Verma, Sai Pranav, Resources- Jatin Bhatt, Juhi Verma, Abhilasha Jain, Software- Juhi Verma, Sai Pranav Supervision- Jatin Bhatt, Abhilasha Jain Validation- Jatin Bhatt Visualization- Jatin Bhatt Writing - original manuscript draft- Juhi Verma, Sai Pranav Writing - review & editing- Juhi Verma, Sai Pranav, Abhilasha Jain, Jatin Bhatt.

DATA AVAILABILITY

The datasets generated during and/or analysed during the current study are available from the corresponding author on reasonable request.

CODE AVAILABILITY

The code used in this manuscript will be available on the reasonable request.

CONFLICT OF INTEREST

On behalf of all authors, the corresponding author states that there is no conflict of interest.

ETHICAL APPROVAL

This research did not contain any studies involving animal or human participants, nor did it take place on any private or protected areas. No specific permissions were required for corresponding locations.

SUPPLEMENTARY INFORMATION

The online version contains supplementary material available at https://doi.org/10.1007/s11661-024-07339-2.

REFERENCES

1. A.L. Greer: *Mater. Today*, 2009, vol. 12(1–2), pp. 14–22.
2. P. Duwez: *Annu. Rev. Mater. Sci.*, 1976, vol. 6(1), pp. 83–117.
3. A. Inoue: *Mater. Trans. JIM*, 1995, vol. 36, pp. 866–75.
4. W.L. Johnson: *Prog. Mater. Sci.*, 1986, vol. 30(2), pp. 81–134.
5. H.S. Chen: *Acta Metall.*, 1974, vol. 22(11), pp. 1505–11.
6. A.L. Drehman, A.L. Greer, and D. Turnbull: *Appl. Phys. Lett.*, 1982, vol. 41, pp. 716–17.
7. W.H. Kui, A.L. Greer, and D. Turnbull: *Appl. Phys. Lett.*, 1984, vol. 45, pp. 615–16.
8. A. Inoue, T. Zhang, and T. Masumoto: *Mater. Trans. JIM*, 1989, vol. 30, p. 965.
9. D. Turnbull: *Contemp. Phys.*, 1969, vol. 10, pp. 437–88.
10. Z.P. Lu and C.T. Liu: *Acta Mater.*, 2002, vol. 50, p. 3501.
11. Z.P. Lu and C.T. Liu: *Phys. Rev. Lett.*, 2004, vol. 91, pp. 115505–11.
12. A. Inoue, T. Zhang, and T. Masumoto, Mater. Trans. *JIM*, 1990, vol. 31, pp. 177–83 (1990).
13. Z.P. Lu and C.T. Liu: *Acta mater.*, 2002, vol. 50(13), pp. 3501–12.
14. K. Mondal and B.S. Murty: *J. Non-Cryst. Solids*, 2005, vol. 35, pp. 1366–71.
15. J. Bhatt and B.S. Murty: *Mater. Sci. Forum*, 2010, vol. 649, pp. 67–73.
16. A. Inoue: *Acta Mater.*, 2010, vol. 48(1), pp. 279–306.
17. A.L. Greer: *Nature*, 1994, vol. 368(6473), pp. 688–89.
18. A. Khond, D.A. Babu, S. Smarana, A. Deshmukh, B. Majumdar, J. Bhatt, and A.K. Srivastava, J. Non Cryst. Solids, 2018, vol. 500, pp. 191-195 (2018).
19. M.D. Ediger, C.A. Angell, and S.R. Nagel: *J. Phys. Chem.*, 1996, vol. 100, pp. 13200–12.
20. D.M. Lee, J.H. Sun, D.H. Kang, S.Y. Shin, G. Welsch, and C.H. Lee: *Intermetallics*, 2012, vol. 21(1), pp. 67–74.
21. J. Bhatt, J. Kumar, and B.S. Murty: *Mater. Sci. Forum*, 2011, vol. 675(677), pp. 189–92.
22. Y. Prabhu, A.K. Srivastav, D. V. Gunderov, and J. Bhatt, Physica B 2022, vol. 624 (2022).
23. B.S. Rao, J. Bhatt, and B.S. Murty: *Mater. Sci. Eng.*, 2007, vol. 448(451), pp. 211–14.
24. B.R. Rao, A.S. Gandhi, S. Vincent, J. Bhatt, and B.S. Murty: *Trans. Indian Inst. Met.*, 2012, vol. 65, pp. 559–63.
25. K.S.N.S. Idury, B.S. Murty, and J. Bhatt: *Intermetallics*, 2015, vol. 65, pp. 42–50.
26. S. Vincent, B.S. Murty, and J. Bhatt: *Trans. Indian Inst. Met.*, 2012, vol. 65(6), pp. 827–31.

27. A. Khond, D.A. Babu, S. Smarana, A. Deshmukh, B. Majumdar, J. Bhatt, A.K. Srivastava, and J. Non-Cryst: *Solids*, 2018, vol. 500(15), pp. 191–95.
28. Z. Lei, C. Hongmei, O. Yifang, and D.U. Yong: *J. Rare Earths*, 2014, vol. 32, p. 343.
29. S. Hiromoto, A.P. Tsai, M. Sumita, and T. Hanawa: *Corros. Sci.*, 2000, vol. 42, pp. 1651–60.
30. M.L. Morrison, R.A. Buchanan, R.V. Leon, C.T. Liu, B.A. Green, P.K. Liaw, and J.A. Horton, J. Biomed. Mater. Res. A, 2005, vol. 74, pp. 430–38 (2005).
31. G. Chen, J.L. Cheng, and C.T. Liu: *Intermetallics*, 2012, vol. 28, pp. 25–33.
32. M. Chen, A. Inoue, W. Zhang, and T. Sakurai: *Phys. Rev. Lett.*, 2006, vol. 96, 245502.
33. W.H. Wang, Z. Bian, P. Wen, Y. Zhang, M.X. Pan, and D.Q. Zhao: *Intermetallics*, 2002, vol. 10(11–12), pp. 1249–57.
34. D. Wang, Y. Li, B.B. Sun, M.L. Sui, K. Lu, and E. Ma: *Appl. Phys. Lett.*, 2004, vol. 84(20), pp. 4029–31.
35. Q. Zhang, W. Zhang, G. Xie, and A. Inoue: *Mater. Trans.*, 2007, vol. 48(7), pp. 1626–30.
36. A. Inoue and W. Zhang: *Mater. Trans.*, 2002, vol. 43(11), pp. 2921–25.
37. Q.K. Jiang, X.P. Nie, Y.G. Li, Y. Jin, Z.Y. Chang, X.M. Huang, and J.Z. Jiang: *J. Alloys Compd.*, 2007, vol. 443, pp. 191–94.
38. W. Zhang, F. Jia, Q. Zhang, and A. Inoue: *Mater. Sci. Eng. A*, 2007, vol. 459, pp. 330–36.
39. W. Zhang, Q. Zhang, C. Qin, and A. Inoue: *Mater. Sci. Eng. B*, 2008, vol. 148, pp. 92–96.
40. Q. Zhang, W. Zhang, and A. Inoue: *Mater. Trans.*, 2007, vol. 48(3), pp. 629–31.
41. M. Celtek, U. Domekeli, S. Sengul, and C. Canan: *Intermetallics*, 2021, vol. 128, 107023.
42. K. Liang, X. Zhang, J. Qiao, S. Pan, and S. Feng: *J. Non-Cryst. Solids*, 2020, vol. 550, 120385.
43. S. Sanjay, A.P. Srivastava, and S. Neogy: *J. Alloys Compd.*, 2019, vol. 772, pp. 961–67.
44. L.J. Gallego, J. A. Somoza and J. A. Alonso, J. Condens. Matter Phys., 1990, pp. 62-45.
45. A.K. Niessen, F.R. de Boer, R. Boom, P.F. de Chatel, W.C.M. Mattens, and A.R. Miedema: *Calphad*, 1983, vol. 7, pp. 51–70.
46. A. Takeuchi, K. Amiya, T. Wada, K. Yubuta, W. Zhang, and A. Makino: *Entropy*, 2013, vol. 15, pp. 3810–21.
47. G.A. Mansoori, N.F. Carnahan, K.E. Starling, and T.W. Lelanf Jr.: *J. Chem. Phys.*, 1971, vol. 54, pp. 1523–25.
48. G.D. Scott and D.M. Kilgour: *J. Phys. D*, 1969, vol. 2, pp. 863–66.
49. Y. Prabhu, S. Vincent, S. Manulal, A. Nair, and J. Bhatt: *Physica B*, 2021, vol. 609, 412918.
50. A.R. Miedema, P.F. de Chatel, and F.R. de Boer, Phys. B + C, 1980, vol. 100, pp.1–28.
51. Y. Prabhu, S. Vincent, and J. Bhatt: *Mater. Today*, 2020, vol. 28, pp. 1239–44.
52. D. R. Gaskell, and D. E. Laughlin, fifth ed.,(CRC Press, Germany, 2017) pp. 29–35.
53. H.S. Chen: *Acta Metall.*, 1976, vol. 24(2), pp. 153–58.
54. J. Bhatt, W. Jiang, X. Junhai, W. Qing, C. Dong, and B.S. Murty: *Intermetallics*, 2007, vol. 15, pp. 716–21.
55. S. Vincent, D.R. Peshwe, B.S. Murty, and J. Bhatt: *J. Non Cryst. Solids*, 2011, vol. 357, pp. 3495–99.
56. J. Guo, X. Bian, X. Li, and C. Zhang: *Intermetallics*, 2010, vol. 18, pp. 933–37.
57. A.J. Drehman and A.L. Greer: *Acta Metall.*, 1984, vol. 32(3), pp. 323–32.
58. E. Perim, D. Lee, Y. Liu, C. Toher, P. Gong, Y. Li, W.N. Simmons, O. Levy, J.J. Vlassak, J. Schroers, and S. Curtarolo: *Nat. Commun.*, 2016, vol. 7, p. 12315.
59. D.B. Miracle, W.S. Sanders, and O.N. Senkov: *Philos. Mag.*, 2003, vol. 83(20), pp. 2409–28.
60. A. Takeuchi and A. Inoue: *Mater. Trans. JIM*, 2000, vol. 41, p. 13728.
61. J.D. Lee, 4th ed. (Chapman and Hall, New York, 1991) pp. 146–48.
62. Q.K. Jiang, X.D. Wang, X. P. Nie, G.Q. Zhang, H. Ma, H.J. Fecht, J. Bendnarcik, H. Franz, Y.G. Liu, Q.P. Cao, and J. Z. Jiang, Acta Mater., 2008, vol. 1-56(8), pp. 1785–96 (2008).
63. B.R. Rao, A.K. Shah, M. Srinivas, J. Bhatt, A.S. Gandhi, and B.S. Murty: *Metall. Mater. Trans. A*, 2011, vol. 42, pp. 3913–20.
64. J. Bhatt, G. Dey, and B.S. Murty: *Metall. Mater. Trans. A*, 2008, vol. 39, pp. 1543–51.
65. J. Bhatt and B.S. Murty: *Trans. IIM*, 2009, vol. 62, pp. 413–16.
66. G.Q. Zhang, Q.K. Jiang, L.Y. Chen, M. Shao, J.F. Liu, and J.Z. Jiang: *J. Alloys Compd.*, 2006, vol. 424, pp. 176–78.
67. R. Yuan, Z. Yu, H. Leng, and K. Chou: *J. Non Cryst. Solids*, 2021, vol. 564, 120835.
68. J. Xiong, S.Q. Shi, and T.Y. Zhang: *Mater. Des.*, 2020, vol. 187, 108378.
69. J. Verma, P. Bohane, J. Bhatt, and A.K. Srivastava: *Non-cryst. Solids*, 2015, vol. 624, 122710.
70. S. Vincent, B.S. Murty, and J. Bhatt: *Trans of the IIM*, 2012, vol. 65, pp. 827–31.
71. K.S.N. Satish Idury, and J. Bhatt, Proceedings of 6thICTACEM 2014.
72. Y. Prabhu, S. Vincent, A. Nair, W. Kim, E.S. Park, and J. Bhatt: *Metall. Mater. Trans. A*, 2022, vol. 53, pp. 1419–29.
73. B.R. Rao, M. Srinivas, A.K. Shah, A.S. Gandhi, and B.S. Murty: *Intermetallics*, 2013, vol. 35, pp. 73–81.
74. C. Chattopadhyay, K. S. N. S. Idury, J. Bhatt, K. Mondal, and B. S. Murty, Mate. Sci. Technol., 2015, vol. 34, pp. 380–400.
75. D. Sung, O. Kwon, E. Fleury, K. Kim, J. Lee, D. Kim, and Y. Kim: *Met. Mater. Int.*, 2004, vol. 10, pp. 575–79.
76. W. Zhang, Q. Zhang, C. Qin, and A. Inoue, Mater. Sci. Eng. B, 2008, vol. 148, pp. 92–96 (2008).
77. D.A. Yagodin, V.A. Bykov, T.V. Kulikova, T.V. Shunyaev, S.K. Estemirova, and R.E. Ryltsev, Mater. Res. Express, 2018, vol. 6(3), pp. 036510.
78. A. Inoue, ed. By A. Inoue, K. Hashimoto (Springer, Berlin, 2001) pp.1–51.
79. A. Inoue, T. Zhang, and T. Masumoto, J. Non Cryst. Solids, 1993, vol. 156(158), pp. 473–80.
80. T. Egami, and Y. Waseda, J. Non Cryst. Solids, 1984, vol. 64.1(2), pp. 113–34.
81. D. Wang and Y. Li: *Appl. Phys. Lett.*, 2004, vol. 84(20), pp. 4029–31.
82. Y. Wu, H. Wang, H.H. Wu, Z.Y. Zhang, X.D. Hui, G.L. Chen, D. Ma, X.L. Wang, and Z.P. Lu, Acta. Mater, 2011, vol. 59(8), pp. 2928–26.
83. Z.D. Sha and Q.X. Pei: *Alloys Compd.*, 2015, vol. 619, pp. 16–19.